Research on Engineering Structures & Materials
www.jresm.org

Regional wind-energy suitability screening under uncertainty using GIS-MCDA in Kayseri, Türkiye

Talha Taşkanat

Online Publication Date: 05 October 2026

URL: http://www.jresm.org/archive/resm2026-2187en0929rs.html
DOI: http://dx.doi.org/10.17515/resm2026-2187en0929rs

Journal Abbreviation: *Res. Eng. Struct. Mater.*

To cite this article
Taşkanat T. Regional wind-energy suitability screening under uncertainty using GIS-MCDA in Kayseri, Türkiye. *Res. Eng. Struct. Mater*., 2026; 12(5): 3159-3174.

Disclaimer
All the opinions and statements expressed in the papers are on the responsibility of author(s) and are not to be regarded as those of the journal of Research on Engineering Structures and Materials (RESM) organization or related parties. The publishers make no warranty, explicit or implied, or make any representation with respect to the contents of any article will be complete or accurate or up to date. The accuracy of any instructions, equations, or other information should be independently verified. The publisher and related parties shall not be liable for any loss, actions, claims, proceedings, demand or costs or damages whatsoever or howsoever caused arising directly or indirectly in connection with use of the information given in the journal or related means.

Published articles are freely available to users under the terms of Creative Commons Attribution - NonCommercial 4.0 International Public License, as currently displayed at here (the "CC BY - NC").

Research on Engineering Structures & Materials
www.jresm.org
MIM Research Group

Research Article

Regional wind-energy suitability screening under uncertainty using GIS-MCDA in Kayseri, Türkiye

Talha Taşkanat [*,a]

Department of Geomatics Engineering, Erciyes University, Türkiye

Article Info

Article History:

Received 13 Aug 2026

Accepted 29 Sep 2026

Keywords:

Wind energy siting;
Spatial uncertainty;
Land-cover screening;
GIS-MCDA

Abstract

Regional wind energy planning requires spatial screening methods that account for modelling uncertainty before candidate areas advance to detailed investigation. This study presents an uncertainty-aware Geographic Information Systems–Multi-Criteria Decision Analysis framework for onshore wind-energy siting within a Kayseri-centered regional analytical frame in Türkiye. Seven continuous criteria were standardized using an empirical logistic fuzzy approach and evaluated under Equal, CRITIC, and Entropy weighting schemes across permissive, balanced, and strict planning assumptions. A 1000-iteration Monte Carlo simulation was used to examine spatial uncertainty. Within the regional analytical frame, the suitable area decreased from approximately 21,003.5 km^2 under permissive assumptions to 4,946.7 km^2 under strict assumptions. Within the tested perturbation ranges, planning-threshold variation produced a larger mean spatial effect than weight variation. Probability and connectivity rules yielded 31 candidate areas covering approximately 324.0 km^2, and all candidates retained at least 3 km^2 of connected area after LULC-based physical screening. Within the balanced eligible domain, mapped turbine locations showed higher modelled suitability than general eligible background locations (AUC = 0.961), providing an external spatial-consistency diagnostic rather than a measure of predictive accuracy. The resulting candidate areas are intended for detailed investigation and require subsequent legal, ecological, wind-resource, cadastral, engineering, and grid-capacity assessment.

© 2026 MIM Research Group. All rights reserved.

1. Introduction

The transition to renewable energy systems involves regional spatial planning to balance technical requirements with environmental and social constraints [1]. Onshore wind energy siting is a spatial decision problem where resource quality, topographical characteristics, infrastructure accessibility, settlement separation, and ecological protection statuses frequently interact [2,3]. To synthesize these heterogeneous spatial layers, GIS based multi criteria decision analysis (GIS-MCDA) is commonly utilized as a methodological framework for renewable energy facility siting and spatial decision support [4].

However, a methodological challenge remains in the operational interpretation of GIS MCDA outputs. Many regional planning studies produce deterministic suitability surfaces presenting a single map of theoretically favorable locations [5]. While visually informative, these deterministic maps can mask the inherent uncertainties in planning assumptions, criterion weights, and spatial thresholds. When continuous source data are harmonized to a common analytical grid, the resulting cell level score functions as a synthetic planning indicator rather than a definitive engineering parameter. The translation of heterogeneous spatial criteria into structured planning areas requires cautious interpretation and uncertainty assessment [6,7]. If a model is sensitive to

*Corresponding author: talhataskanat@erciyes.edu.tr
[a]orcid.org/0000-0001-6273-9298
DOI: http://dx.doi.org/10.17515/resm2026-2187en0929rs

minor changes in exclusion thresholds or weighting schemes, the resulting high suitability areas require further verification before policy making [8,9]. Therefore, treating uncertainty as an explicit analytical object provides a practical approach to transition from cell level scores to uncertainty characterized candidate areas [10,11].

Türkiye has an expanding renewable energy capacity and a developing body of applied literature on wind energy spatial planning [12,13]. While earlier GIS MCDA applications often focused on the western regions of Türkiye, the complex topography of Central Anatolia also presents notable planning scenarios. The Kayseri and Erciyes regional geospatial context is defined by high environmental heterogeneity, incorporating the volcanic terrain of Mount Erciyes, widespread agricultural lowlands, and expanding settlement corridors, which provides a relevant setting for multi-criteria geospatial screening [14,15]. Although localized studies have evaluated the applicability of GIS methods for wind power planning in this regional setting [16,17], there remains a need for a regional framework that systematically assesses model uncertainty before candidate areas are advanced for detailed investigation.

To address this context, this study presents an uncertainty-aware GIS-MCDA framework for onshore wind-energy siting in a Kayseri-centered regional setting in Türkiye. The study contributes in three ways. First, it combines empirical logistic fuzzy standardization with Equal, CRITIC, and Entropy weighting under permissive, balanced, and strict planning assumptions. Second, it links pixel-level probability surfaces with connected-patch extraction and exact candidate-level Monte Carlo metrics rather than relying only on regional raster summaries. Third, it separates raster suitability modelling from candidate-level prioritization, land-cover characterization, and an external mapped-turbine spatial-consistency diagnostic. A related question is whether spatial uncertainty within the evaluated framework is affected more strongly by variation in criterion weights or by variation in planning-constraint thresholds over the perturbation ranges examined. The resulting framework narrows the regional search space while retaining explicit information on uncertainty for subsequent field, legal, ecological, engineering, and grid-capacity investigations.

2. Materials and Spatial Framework

2.1 Study Area and Environmental Context

The study focuses on Kayseri in central Türkiye and uses a regional analytical frame centered on the province and its immediate surroundings. The Kayseri provincial boundary provides the principal geographic reference, whereas raster-based calculations were performed over the surrounding analytical frame rather than being clipped to the administrative boundary. The regional setting is heterogeneous, comprising high-altitude volcanic topography, extensive agricultural plains, and developing urban and industrial corridors. This setting requires wind-resource conditions to be considered together with terrain, settlement, infrastructure, hydrological, and environmental factors.

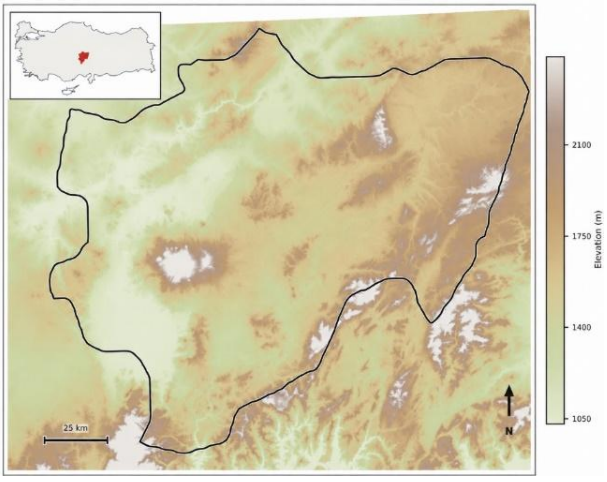

Fig. 1. Location and topographic map of Kayseri within the regional analytical frame

To ensure spatial consistency across all analyses, spatial inputs were transformed to WGS 84 / UTM zone 36N and aligned to the 27 m reference grid established during the preprocessing workflow. The 27 m cell size was retained as an operational harmonization grid rather than as an optimized representation of source resolution. A common-valid data mask excluded cells lacking required aligned inputs and yielded approximately 33,399.3 km^2 within the regional analytical frame. The common grid provides a consistent raster lattice for overlay and spatial calculation; resampling coarser datasets to this grid does not increase their native information content or original spatial detail[18]. Candidate boundaries are therefore interpreted as regional screening geometries rather than engineering-precision site limits. The geographical context and analytical frame are shown in Figure 1.

2.2 Spatial Datasets and Harmonization

The spatial analysis used resource, terrain, infrastructure, settlement, hydrological, environmental, and land-cover datasets. Seven continuous layers entered the WLC suitability calculation: 100 m wind speed, slope, road distance, residential distance, protected-area distance, river distance, and powerline distance. The remaining datasets served as topographic support, preprocessing/context layers, candidate-level screening inputs, or external diagnostic data. Their analytical roles are summarized in Table 1.

Table 1. Spatial datasets and analytical roles.

Input	Source framework	Documented native characteristic	Role in analysis
Wind speed at 100 m	Global Wind Atlas 3.0	~250 m	Continuous resource criterion
Elevation	SRTM DEM	90 m	Topographic support and source for slope; not an independent weighted criterion
Slope	Derived from SRTM DEM	90 m source; 27 m analytical	Continuous terrain criterion
Road distance	OpenStreetMap road vectors	vector source	Euclidean distance criterion
River distance	DSİ surface water data	vector/source dependent	Euclidean distance criterion
Residential distance	HGK settlement data	vector/source dependent	Settlement separation criterion
Substation distance	KCETAŞ/TEİAŞ source framework	vector/source dependent	Ancillary electrical-infrastructure context and common-valid coverage support; not included in WLC or threshold scenarios
Powerline distance	TEİAŞ source framework	vector/source dependent	Electrical infrastructure proximity criterion
Fault distance	MTA active fault data	vector/source dependent	Ancillary planning-context and common-valid coverage support; not included in WLC or threshold scenarios
Protected area distance	TUCBS environmental status data	vector/source dependent	Planning constraint and distance context
ESA WorldCover 2021 v200	European Space Agency	~10 m native	Candidate prioritization screening variables
LULC	CORINE Land Cover-derived local 11-class reclassification [19]	Locally supplied 10 m raster derived from CORINE Land Cover classes; harmonized to 27 m	Candidate-level physical characterization and screening; not included in final composite ranking

The wind resource input was represented by the Global Wind Atlas 3.0 100 m wind speed product [20–22]. Topographical inputs were derived from the SRTM Digital Elevation Model [23–25]. Infrastructure and proximity data were compiled from various national and open-source frameworks [26–28]. The locally reclassified 11-class LULC raster was derived from CORINE Land Cover categories [19].

3. Methodology

The methodology was structured as a sequential spatial screening framework that linked criterion standardization, scenario-based suitability modelling, uncertainty assessment, and candidate-area delineation. Raster-based outputs were subsequently translated into connected candidate units for candidate-level prioritization and land-cover characterization. External mapped-turbine information was evaluated separately as a spatial-consistency diagnostic and was not used in candidate scoring. The overall analytical workflow is summarized in Figure 2.

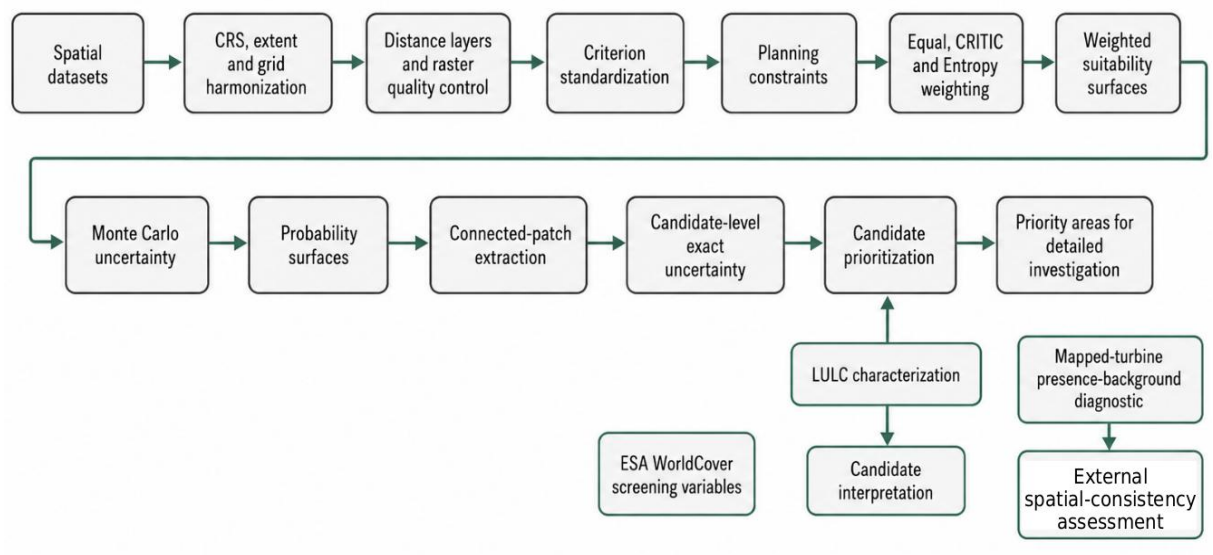

Fig. 2. Data-processing and analytical framework of the study

3.1 Suitability Modelling and Weighting Schemes

Prior to criteria aggregation, an empirical logistic fuzzy standardization was applied to transform physical and distance parameters into dimensionless suitability scores (x_{ij}^{*}) ranging from 0 to 1. Values were initially clipped to their empirical 1st and 99th percentiles ($P1_j$, $P99_j$). The logistic midpoint was set to the empirical median ($P50_j$), and the logistic slope (k_j) was formulated as $k_j = \ln(9) / \text{mean}\left(|P90_j - P50_j|, |P50_j - P10_j|\right)$.

Criteria that prioritize higher values or greater distances (fuzzy large), specifically 100 m wind speed, residential distance, protected-area distance, and river distance, were transformed using Eq. (1).

$$x_{ij}^{*} = \frac{1}{1 + exp\left[-k_j\left(clip\left(x_{ij}, P1_j, P99_j\right) - P50_j\right)\right]} \tag{1}$$

Criteria that prioritize proximity or lower values (fuzzy small) specifically slope, road distance, and powerline distance were transformed using Eq. (2).

$$x_{ij}^{*} = 1 - \frac{1}{1 + exp\left[-k_j\left(clip\left(x_{ij}, P1_j, P99_j\right) - P50_j\right)\right]} \tag{2}$$

Table 2. Empirical logistic standardization parameters used for the seven continuous criteria

Criterion	P1	P10	P50	P90	P99	k_j
Wind speed at 100 m	3.058	4.143	5.491	7.259	9.482	1.410
Slope	0.583	1.538	6.875	22.753	35.458	0.207
Road distance	2.550	43.735	448.185	2295.635	4985.466	1.951×10^{-3}
Residential distance	0.000	779.953	3270.818	9801.677	18262.133	4.87×10^{-4}
Protected-area distance	0.000	1645.929	9180.945	40173.778	69875.966	1.14×10^{-4}
River distance	0.0003	86.532	566.397	1455.398	2245.749	3.210×10^{-3}
Powerline distance	93.964	1386.616	9878.549	34160.713	49095.573	1.34×10^{-4}

The empirical percentiles and logistic-slope parameters were calculated once over the common-valid analytical domain using finite, non-NoData criterion cells and were held fixed during the Monte Carlo simulations. The wind-percentile lookup used for planning constraints was handled separately from these standardization parameters.

For slope and setback-type constraints, scenario values were selected as literature-informed planning assumptions spanning relatively permissive to more restrictive regional screening conditions [8,9,29–31]. These values are not presented as statutory setback requirements for Türkiye. Wind constraints were defined separately using empirical percentiles (P10, P25, and P40) calculated from the aligned wind raster. These percentiles represent relative resource-screening levels within the analytical frame rather than turbine cut-in speeds, economic viability thresholds, or regulatory limits. Road and powerline distances were retained as continuous preference criteria rather than Boolean exclusion constraints because they represent regional accessibility and grid-proximity considerations; their fuzzy-small functions do not represent project-scale engineering clearances or statutory safety setbacks. The scenario thresholds and corresponding suitable areas within the analytical frame are reported in Table 3.

Table 3. Planning assumptions, permissive, balanced, and strict thresholds, and suitable areas within the analytical frame

Constraint	Permissive	Balanced	Strict
Wind empirical percentile	P10	P25	P40
Slope	≤20°	≤15°	≤10°
Residential distance	≥500 m	≥1000 m	≥1500 m
Protected area distance	≥500 m	≥1000 m	≥2000 m
River distance	≥100 m	≥300 m	≥500 m
Suitable area within analytical frame (km^2)	21,003.5	11,508.7	4,946.7

The cell level suitability score (S_i) was calculated using a Weighted Linear Combination approach [2,29]. The standardized values of the seven continuous criteria were aggregated based on their assigned weights (w_j), as shown in Eq. (3). The seven standardized criterion rasters constituted the continuous spatial inputs to the WLC suitability calculation.

$$S_i = \sum_{j=1}^{n} w_j \, x_{ij}^{*} \tag{3}$$

To evaluate structural dependencies within the model, three distinct weighting schemes were compared. Equal Weight was assigned as a transparent baseline reference weighting scheme. CRITIC (Criteria Importance Through Intercriteria Correlation) and Entropy were utilized as data derived objective weighting schemes [32]. The specific criterion weights for each method are summarized in Table 4.

Table 4. Equal, CRITIC, and Entropy weights with model agreement and robustness diagnostics

Criterion or Diagnostic	Equal	CRITIC	Entropy
100 m wind speed	0.142857	0.147767	0.141387
Slope	0.142857	0.146794	0.198838
Road distance	0.142857	0.136978	0.183799
Residential distance	0.142857	0.143987	0.094372
Protected area distance	0.142857	0.139745	0.075635
River distance	0.142857	0.141417	0.121330
Powerline distance	0.142857	0.143314	0.184640
Highest pairwise Spearman	0.9996		
Lowest relevant pairwise Spearman	0.814		
Alternative transformation median Spearman	0.966		
Criterion set robustness median Spearman	0.928		
Balanced Moran's I	0.891		

Weighting method agreement was assessed using pairwise Spearman rank correlations. Transformation robustness and criterion set robustness were summarized from the corresponding sensitivity comparisons, whereas Moran's I was used to characterize global spatial autocorrelation of the balanced suitability surface. Global Moran's I for the balanced ensemble suitability surface was calculated after 10 × 10 block-mean aggregation to 270 m cells using binary queen-contiguity neighbors among finite aggregated cells. Significance was evaluated with 199 random permutations using seed 42.

The primary reporting ensemble was computed as the cell wise arithmetic mean of the three weighting-based suitability surfaces under the balanced planning assumptions. Furthermore, a robust high suitability category was defined to identify a comparatively stable high suitability subset across the evaluated weighting formulations, conceptualized as areas that simultaneously fall within the ensemble mean top 10 percent, the model standard deviation bottom 25 percent, and the top 20 percent of all three individual weighting models.

3.2 Monte Carlo Simulation for Uncertainty Assessment

To transition from a deterministic framework to a probabilistic one, a 1000 iteration Monte Carlo simulation (random seed 42) was executed across three modes: weight-only, threshold-only, and combined. Weight uncertainty was represented using empirical bootstrap weight vectors. For each of the CRITIC and Entropy methods, 500 bootstrap replicates were generated by sampling 50,000 rows with replacement from the common-valid standardized criterion sample using random seed 42. The seven criteria were resampled jointly within each replicate, and the corresponding CRITIC or Entropy weights were recomputed. The stored bootstrap vectors were subsequently sampled during the Monte Carlo simulations. CRITIC and Entropy vectors were selected with probabilities of 0.45 each, while the Equal Weight reference vector was retained with probability 0.10; these probabilities were prespecified simulation-design choices rather than empirically calibrated probabilities. After selection, individual weights were clipped to 0.02–0.35 and renormalized to sum to 1.

For threshold uncertainty, constraint boundaries were varied independently using triangular probability distributions (lower, mode, upper), a bounded form commonly used to represent uncertain parameter ranges [11]. The scenario-specific bounds were prespecified for this study and were not interpreted as regulatory tolerances or measurement-error distributions; symmetry around the mode was not imposed. The distributions were: slope (permissive 16, 20, 24°; balanced 12, 15, 18°; strict 8, 10, 12°); residential distance (400, 500, 700 m; 750, 1000, 1250 m; 1250, 1500, 2000 m); protected-area distance (400, 500, 750 m; 750, 1000, 1500 m; 1500, 2000, 2500 m); and river distance (75, 100, 150 m; 200, 300, 400 m; 400, 500, 700 m). Wind uncertainty used empirical percentile triplets (5, 10, 15; 20, 25, 30; 35, 40, 45) applied through the aligned wind-raster percentile lookup. The combined mode varied weights and thresholds simultaneously. Because the

uncertainty modes use different perturbation ranges and distributional forms, comparisons between their effects are conditional on this simulation design.

To accurately represent eligibility uncertainty, an explicit zero handling approach was implemented. If a cell was ineligible in a given iteration, its suitability contribution was recorded as 0. Consequently, the full resolution Monte Carlo suitability mean and standard deviation products, as well as the bounded moment-based approximations (P05, P10, median, P90, and P95), are unconditional suitability moments that incorporate eligibility uncertainty. They are not exact empirical Monte Carlo quantiles. Exact empirical quantiles were calculated exclusively for candidate level Monte Carlo summaries. Suitability outcomes were quantified through explicit probability metrics. The eligibility probability ($P_{E,i}$) measures the proportion of all iterations (R) in which cell i remained eligible ($E_{ir} = 1$), shown in Eq. 4.

$$P_{E,i} = \frac{1}{R}\sum_{r=1}^{R} I\,(E_{ir} = 1) \tag{4}$$

Monte Carlo suitability uncertainty (U_i) was calculated as the standard deviation of suitability scores across the 1000 iterations, where $\bar{S}_i$ denotes the cell mean (Eq. (5)).

$$U_i = \sqrt{\frac{1}{R}\sum_{r=1}^{R}(S_{ir} - \bar{S}_i)^2} \tag{5}$$

High suitability events were defined separately for each Monte Carlo iteration, uncertainty mode, and planning scenario. For iteration r, the high suitability threshold (τ_r) was defined as the 90th percentile of suitability scores among eligible sampled cells. This dynamic score threshold must not be confused with the 0.75 probability cutoff utilized later for candidate extraction. To distinguish between the persistence of inclusion and the persistence of high scores, conditional and unconditional high suitability probabilities were evaluated. The conditional high suitability probability ($P_{C,i}$) evaluates high suitability solely across eligible iterations (Eq. (6)), whereas the unconditional high suitability probability ($P_{U,i}$) evaluates the proportion across all iterations (Eq. (7)).

$$P_{C,i} = \frac{\sum_{r=1}^{R} I\,(E_{ir} = 1 \wedge S_{ir} \geq \tau_r)}{\sum_{r=1}^{R} I\,(E_{ir} = 1)} \tag{6}$$

$$P_{U,i} = \frac{1}{R}\sum_{r=1}^{R} I\,(E_{ir} = 1 \wedge S_{ir} \geq \tau_r) \tag{7}$$

3.3 Candidate Extraction and Diagnostic Screening

Connected-patch extraction was applied to the balanced planning assumption under the combined uncertainty mode to translate pixel-level probabilities into regional planning units. Candidate cells were required to have both eligibility probability ≥ 0.75 and conditional high-suitability probability ≥ 0.75 across finite, non-NoData cells; unconditional high-suitability probability and raw suitability scores were not used directly in this mask. Morphological cleanup removed eligible components smaller than 10 ha and subsequently filled internal holes smaller than 10 ha using 8-neighbour connectivity (138 pixels on the 27 m grid). Following cleanup, connected components were extracted and a minimum connected area of 5 km^2 was applied as a prespecified operational regional-screening threshold. This threshold was used to remove small fragmented patches and was not treated as a universal minimum wind-farm area.

Exact empirical quantiles and high suitability fractions were calculated for the extracted candidate polygons. Candidate level iteration statistics were calculated only if at least one eligible candidate pixel existed; in iterations with no eligible pixels, suitability summaries were recorded as NaN, and candidate level suitability quantiles were calculated over the finite iteration means. The candidate level exact high suitability fraction represents the Monte Carlo mean of the fraction of valid

candidate pixels meeting the eligibility and iteration specific high suitability conditions; it is therefore distinct from the cell level conditional probability raster.

Final candidate ordering relied on a composite prioritization score rather than exact Monte Carlo rank alone. The exact Monte Carlo robustness sub component (R_i) was formulated as Eq. (8), where mm denotes min max normalization across the candidate set.

$$R_i = 0.45 \times mm(P10_i) + 0.35 \times mm\left(P_{high,i}\right) + 0.20 \times mm(-SD_i) \tag{8}$$

The final composite priority score (C_i) combined exact Monte Carlo robustness (R_i), normalized log remaining connected area (A_i), ESA WorldCover-based land-cover compatibility (L_i), baseline aggregate suitability (B_i), and scenario persistence (P_i), as shown in Eq. (9). The component coefficients were prespecified as part of the candidate-prioritization rule and were not optimized against mapped turbine locations or other external outcomes.

$$C_i = 0.285714 \times R_i + 0.214286 \times A_i + 0.214286 \times L_i + 0.214286 \times B_i + 0.071429 \times P_i \tag{9}$$

Here, A_i is the min-max normalized log1p of the largest remaining connected component derived from ESA WorldCover screening, and L_i = 1 − excluded fraction using ESA WorldCover classes 50 (built-up), 70 (snow and ice), 80 (permanent water), 90 (herbaceous wetland), and 95 (mangroves). B_i is the clipped primary baseline aggregate suitability score, and P_i is the stable-scenario count divided by three. Data-support class was retained as descriptive metadata (A = 1.0, B = 0.8, C = 0.5, D = 0.2). Because all 31 candidates were assigned class C, the data-support term was constant and was therefore removed from the ranking equation; the remaining coefficients were renormalized to sum to one. This affine rescaling does not alter candidate ordering.

3.4 LULC Characterization and OSM Diagnostic

Two land-cover datasets served different candidate-level roles. ESA WorldCover 2021 v200 supplied screening variables incorporated into the composite candidate-prioritization score. A separate 11-class LULC raster derived through local reclassification of CORINE Land Cover categories [19] was used for candidate-level physical characterization and screening. The CORINE-derived raster did not enter the final composite ranking.

External spatial consistency was examined using mapped wind-energy infrastructure from OpenStreetMap. The inventory contained 288 deduplicated turbine features; 163 were outside the analysis raster extent and 15 did not satisfy the balanced-domain eligibility mask, leaving 110 locations with finite model values for the primary diagnostic. These 110 points were compared with 2,200 general eligible background locations sampled from the balanced planning domain outside a 2 km turbine buffer. A second 2,200-point background matched by wind and slope deciles was used as a sensitivity comparison. No filtering was based on candidate rank or high-suitability outcome. Because the final presence sample was conditioned on the balanced eligible domain, the comparison is interpreted as an external spatial-consistency diagnostic within that domain rather than as independent predictive validation. OSM information was not used in candidate scoring.

4. Results

4.1 Spatial Suitability and Inter-model Disagreement

Planning constraints reduced the eligible search domain within the regional analytical frame. As reported in Table 3, suitable area was approximately 21,003.5 km^2 under permissive assumptions, 11,508.7 km^2 under balanced assumptions, and 4,946.7 km^2 under strict assumptions.

Under the balanced assumptions, pairwise rank correspondence among the weighting formulations ranged from Spearman ρ = 0.814 to 0.9996, with the highest agreement between Equal and CRITIC. The primary reporting ensemble represented the shared spatial tendency while retaining information on inter-model disagreement. The balanced top-10% consensus area

covered approximately 755.5 km² (Figure 3c), and the robust-high subset covered 395.4 km² (Figure 3d).

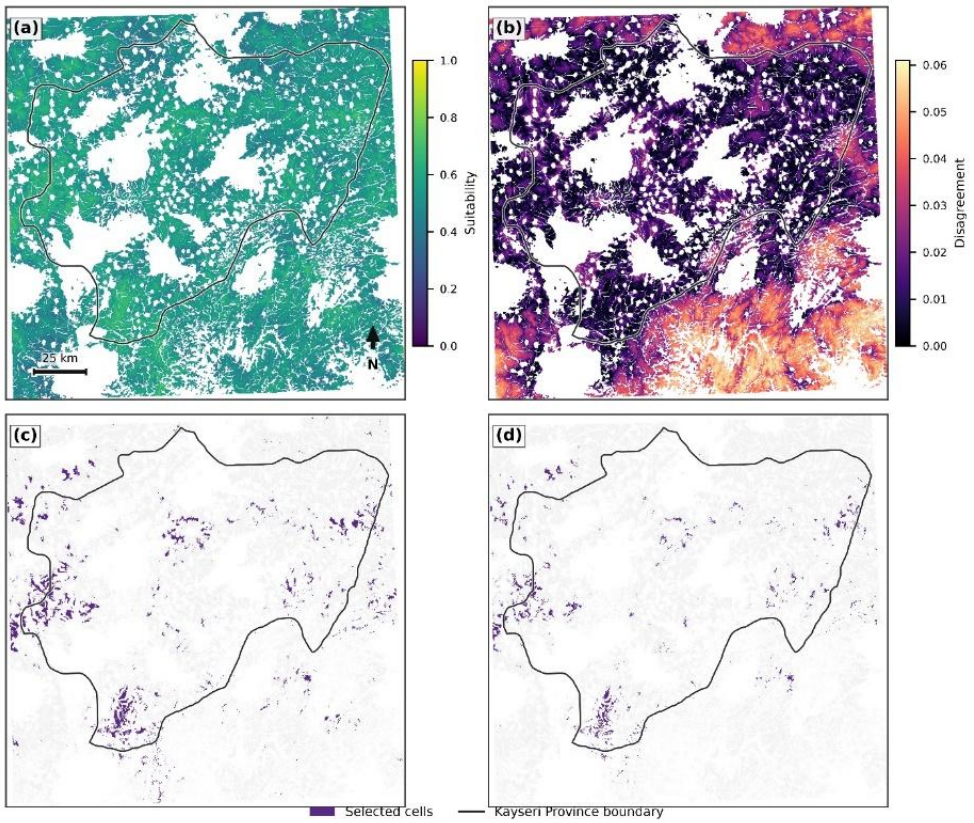

Fig. 3. Balanced ensemble suitability and robustness surfaces: (a) mean suitability, (b) inter-model disagreement, (c) top-10% consensus, and (d) robust-high suitability.

4.2 Probability Surfaces and Impact of Threshold Uncertainty

Within the tested perturbation ranges, the Monte Carlo simulation produced a larger mean spatial effect under threshold-only perturbation than under weight-only perturbation. Mean spatial uncertainty was 0.006 for weight-only perturbation, 0.035 for threshold-only perturbation, and 0.039 for the combined mode.

An eligibility probability ≥ 0.90 was identified across approximately 9,491.7 km² (Figure 4c). Conditional high-suitability probability ≥ 0.90 covered 766.9 km² (Figure 4d), whereas the corresponding unconditional probability ≥ 0.90 covered 710.4 km². These surfaces distinguish persistence of eligibility from persistence of high suitability under the sampled uncertainty settings.

4.3 Priority Candidate Areas and Exact Metrics

The initial patch extraction identified 14,902 raw connected components, which were reduced to 560 after morphological cleanup. Retained patch counts were 143 at ≥1 km², 69 at ≥2 km², 31 at ≥5 km², 12 at ≥10 km², and 2 at ≥20 km². Applying the prespecified ≥5 km² regional-screening threshold yielded 31 candidate areas covering approximately 324.0 km², with the largest patch covering 31.00 km².

The median absolute difference between exact and approximate candidate-level P10 values was 0.008. Baseline aggregate rank and exact Monte Carlo rank showed moderate correspondence (Spearman ρ = 0.644), indicating sensitivity of candidate ordering to the selected candidate-level uncertainty summary. The top 10 areas according to the final composite priority score are reported in Table 5; eight were persistent across all three planning scenarios, while KAY-WIND-006 and KAY-WIND-005 were persistent in two of three.

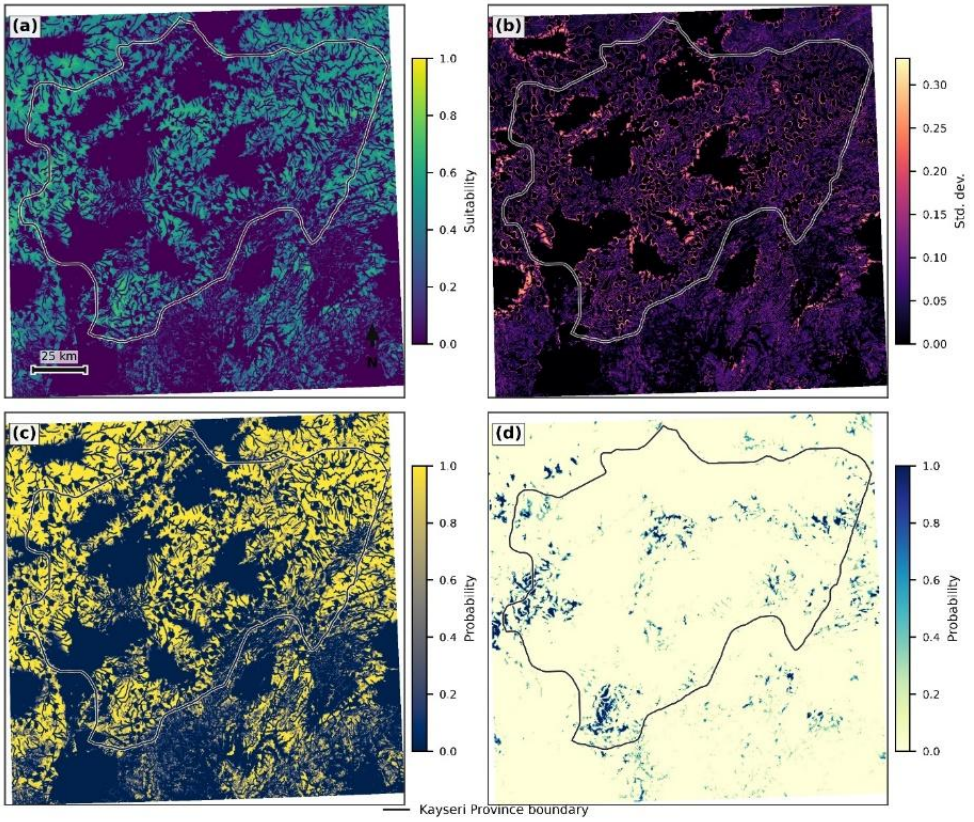

Fig. 4. Monte Carlo uncertainty and probability products for the balanced planning assumption set: (a) mean suitability, (b) combined uncertainty, (c) eligibility probability, and (d) conditional high-suitability probability.

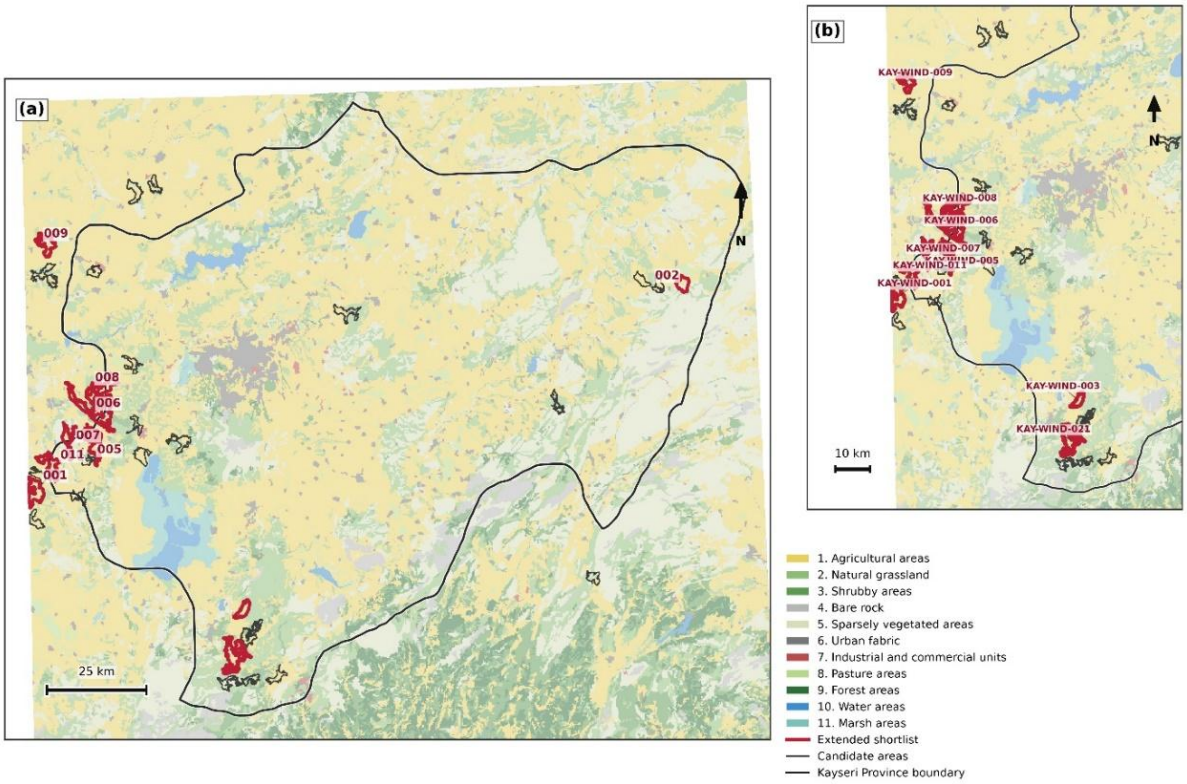

Fig. 5. Priority candidate areas and LULC context: (a) regional distribution of candidate areas with the Kayseri provincial boundary shown for geographic reference and the extended shortlist; (b) enlarged view of the main candidate concentration.

Table 5. Top 10 candidate areas according to the final composite prioritization score, with selected exact candidate-level Monte Carlo and LULC characterization metrics

Rank	Candidate	Area (km^2)	Exact P10	Exact high fraction	Exact MC SD	Final score	LULC / conflict
1	KAY-WIND-006	31.00	0.678	0.988	0.002	0.8793	Natural grassland / None
2	KAY-WIND-001	16.29	0.682	0.992	0.001	0.8717	Agricultural / None
3	KAY-WIND-005	16.90	0.671	0.994	0.004	0.7967	Agricultural / None
4	KAY-WIND-008	16.31	0.669	0.989	0.006	0.7823	Agricultural / None
5	KAY-WIND-003	7.95	0.682	0.991	0.003	0.7745	Agricultural / None
6	KAY-WIND-002	8.28	0.685	0.987	0.005	0.7664	Sparsely vegetated / Industrial-commercial
7	KAY-WIND-011	13.95	0.666	0.989	0.002	0.7509	Agricultural / None
8	KAY-WIND-021	24.44	0.679	0.960	0.003	0.7505	Natural grassland / None
9	KAY-WIND-007	9.90	0.675	0.988	0.004	0.7474	Agricultural / None
10	KAY-WIND-009	12.83	0.672	0.983	0.005	0.7209	Agricultural / Industrial-commercial

The CORINE-derived 11-class LULC characterization identified agriculture as the dominant class in 24 candidates, natural grassland in 4, sparsely vegetated land in 2, and shrubland in 1. All 31 candidates retained at least 3 km^2 of connected area after the physical screening; this was an observed outcome rather than an additional methodological threshold. No urban-fabric or water conflicts were identified. Industrial or commercial conflicts occurred in six candidates, and a marsh conflict occurred in KAY-WIND-004. KAY-WIND-009 showed the largest absolute screened-area loss (1.59 km^2; 12.4%). Differences between ESA WorldCover and the CORINE-derived LULC raster were retained as a thematic-data limitation because the products use different classification and spatial representations. Candidate distribution and LULC context are shown in Figure 5.

4.4 External Spatial Consistency with Mapped Wind Turbines

The mapped-turbine diagnostic began with 288 deduplicated OSM features and retained 110 valid presence locations within the balanced eligible analysis domain. These locations represented 14 spatial clusters. Three candidate areas contained mapped turbines, and six candidates were within 5 km of mapped turbines.

The primary presence-background comparison yielded a balanced-ensemble AUC of 0.961 (permutation $p = 0.001$), and 98 of 110 valid mapped-turbine locations (89.1%) occurred above the general-background 90th percentile. The presence and background medians were 0.675 and 0.538, respectively (Figure 6b). The Monte Carlo mean-surface AUC against the general background was 0.888.

The wind- and slope-decile matched background produced a lower AUC of 0.890, indicating that part of the primary separation was associated with wind and terrain gradients represented in the suitability model. A cluster-representative sensitivity analysis using nine valid representatives yielded an AUC of 0.947 against the general eligible background and 0.868 against the matched background. These results are summarized in Table 6 and the primary presence-background distributions are shown in Figure 6b.

Table 6. Mapped-turbine presence-background spatial-consistency diagnostic results

Diagnostic Metric	Value	Interpretation
Mapped turbine inventory	288	Deduplicated OSM features
Valid presence points	110	Locations retained within the balanced eligible domain
Spatial clusters identified	14	Cluster assessment
Valid cluster representatives	9	Used in cluster-representative sensitivity comparison
General background points	2,200	Primary eligible background sample
Presence median (balanced)	0.675	Compared with primary background median
Background median (balanced)	0.538	Primary general eligible background
Presence-background AUC	0.961	Primary balanced-ensemble spatial-consistency diagnostic
Valid presence points above general background P90	98/110 (89.1 percent)	Balanced ensemble top decile evaluation
Matched-background AUC	0.890	Wind/slope-decile matched sensitivity comparison
Monte Carlo mean-surface AUC	0.888	General-background comparison
Cluster-representative AUC (general)	0.947	Nine valid cluster representatives
Cluster-representative AUC (matched)	0.868	Nine valid cluster representatives; matched background

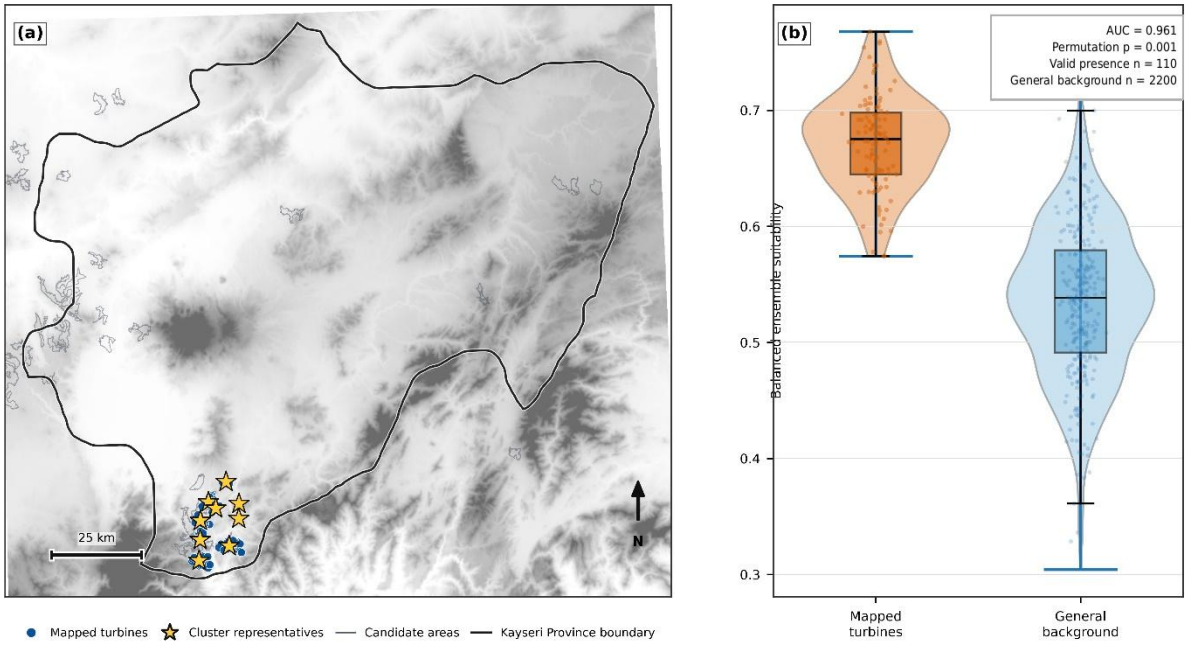

Fig. 6. Mapped-turbine external spatial-consistency diagnostic: (a) mapped-turbine locations, cluster representatives, candidate areas, (b) suitability distributions for mapped-turbine presence and general background locations.

5. Discussion

5.1 Relative Effects of Threshold and Weight Uncertainty

An analytical outcome of this framework is the relative impact of threshold uncertainty compared to criterion weight uncertainty. In the broader GIS MCDA literature, investigations frequently emphasize the refinement of criteria weights as a method to ensure reliability [4,32]. However, the

1000-iteration Monte Carlo simulation showed that within the tested perturbation ranges, variation in planning thresholds produced a substantially larger mean spatial effect than variation in criterion weights. Because the weight and threshold modes were assigned different perturbation ranges and distributional forms, the magnitude of this contrast is conditional on the adopted simulation design and should not be interpreted as a general ordering of threshold and weight uncertainty in GIS-MCDA studies.

This outcome indicates that variations in Boolean planning constraints such as adjusting the setback distance from residential zones or riverbeds can shift substantial areas between eligible and excluded states [30,31]. The methodological ensemble approach accommodates the internal contrast between Equal, CRITIC, and Entropy weights, but analytical effort in regional screening requires explicit justification of the chosen spatial exclusion thresholds, as these exert an influence on spatial availability [9,33].

5.2 Operationalizing Raster Data: From Pixels to Planning Units

A common limitation in regional spatial screening is the reliance on isolated high value raster cells [5]. Isolated high value cells provide limited information as area level planning units because they do not explicitly represent spatially connected candidate geometries. By implementing probability thresholds and connected patch extraction, the model condensed raw raster components into 31 connected candidate areas ($\geq$5 km^2). The 5 km^2 criterion was used as an operational regional-screening threshold to remove small fragmented patches and should not be interpreted as a universal minimum wind-farm size.

Translating raster grids into connected polygons provides discrete planning units for candidate level uncertainty and land cover attributes [34,35]. Their moderate rank correspondence with the baseline aggregate ranking indicates that candidate prioritization may be sensitive to the choice of uncertainty summary. Project-level turbine spacing, rotor diameter, wake effects, installed-capacity density, and micro siting requirements are separate engineering considerations and require site-specific design rather than inference from the regional patch threshold.

5.3 Recontextualizing Land-Cover and Mapped-Turbine Diagnostics

The integration of land-cover information was separated into two candidate-level functions. ESA WorldCover-derived metrics contributed directly to the candidate-prioritization score, whereas the CORINE-derived 11-class LULC raster was used only for physical characterization and screening. Agricultural and pasture-related classes were treated as planning-review signals rather than automatic evidence of legal or project-level suitability. The local 11-class raster was derived from CORINE Land Cover categories [19]. Differences observed between the two land-cover products were retained as a thematic-data limitation because the products use different classification schemes and spatial representations.

The mapped-turbine comparison provides an external spatial-consistency diagnostic within the balanced eligible domain, with a primary presence-background AUC of 0.961. Mapped turbine locations tended to receive higher modelled suitability than the general eligible background, while the lower matched-background AUC (0.890) indicates that part of the contrast reflects wind and slope gradients represented in the suitability model. The diagnostic measures presence-background discrimination rather than predictive accuracy [36]. Background points do not represent true developmental absences, and economic, historical, grid related, and permitting factors may also influence turbine placement [34].

5.4 Limitations and Requirements for Future Investigation

This regional screening framework does not provide project-level engineering clearance. Subsequent project assessment requires locally verified wind-resource information and site-specific resource characterization [37], together with cadastral and parcel verification, ecological assessment, pasture status and any applicable land-use conversion procedures under Pasture Law No. 4342 [38], military and civil aviation constraints including radar and technical-interaction requirements assessed by the competent authorities [39,40], and confirmation of the actual

connection capacity available at the relevant grid node [41]. Spatial proximity to a substation or transmission line does not itself establish grid-connection feasibility.

6. Conclusion

This study developed an uncertainty-aware GIS-MCDA framework for regional onshore wind-energy screening within a Kayseri-centered analytical frame in Türkiye. The analysis combines suitability modelling with scenario-based planning constraints, uncertainty assessment, connected candidate extraction, and candidate-level prioritization. Calculations were performed over a common-valid regional raster frame surrounding Kayseri rather than being clipped to the provincial administrative boundary; consequently, the reported area values refer to the analytical domain rather than the official area of Kayseri Province.

The scenario comparison showed that the extent of eligible land changes materially when planning thresholds are varied. Under the strict assumptions, the suitable area was approximately one quarter of that obtained under the permissive assumptions. Within the perturbation ranges used in this study, threshold-only variation also produced a larger mean spatial effect than weight-only variation. This comparison is conditional on the adopted perturbation ranges and probability distributions and is not intended to establish a universal dominance of threshold uncertainty over weight uncertainty in GIS-MCDA applications.

Probability-based screening and connectivity rules converted the regional raster outputs into 31 connected candidate areas. Candidate prioritization combined exact Monte Carlo robustness, remaining connected area, ESA WorldCover-based land-cover compatibility, baseline suitability, and scenario persistence. The separate CORINE-derived 11-class LULC raster was used for physical characterization rather than ranking, and all candidates retained at least 3 km^2 of connected area after this screening step.

Mapped OSM turbine locations provided a supplementary spatial-consistency check within the balanced eligible domain. Their modelled suitability was higher than that of the general eligible background, with a primary AUC of 0.961. The lower matched-background comparison indicates that part of this separation is associated with wind and slope gradients already represented in the suitability model. Because background locations are not verified development absences and the presence sample is conditioned on model eligibility, this comparison is not a measure of predictive accuracy or project feasibility.

For regional planning, the main contribution of the framework is the distinction between locations that remain comparatively persistent under repeated scenario perturbations and locations whose eligibility or high-suitability status is more sensitive to modelling assumptions. This information can support the sequencing of subsequent field surveys and institutional screening, but the candidate polygons do not constitute approval decisions or engineering-ready wind-farm sites. Site-specific wind measurement, turbine micrositing, cadastral verification, ecological assessment, pasture and land-use procedures, aviation and radar review, and verified grid-connection capacity remain necessary before project-level decisions can be made.

Future work may examine alternative uncertainty ranges and candidate-prioritization formulations, incorporate locally measured wind information and temporally updated grid-capacity data, and assess the transferability of the framework to other regions. Extensions to combined wind-solar planning and to scenarios that consider future changes in wind-resource conditions would also allow the regional screening approach to be evaluated under a wider range of planning contexts.

References

[1] Değirmenci S, Bingöl F, Sofuoglu SC. MCDM analysis of wind energy in Turkey: Decision making based on environmental impact. Environmental Science and Pollution Research. 2018;25(20):19753-19766. https://doi.org/10.1007/s11356-018-2004-4

[2] Ayodele TR, Ogunjuyigbe ASO, Odigie O, et al. A multi-criteria GIS based model for wind farm site selection using interval type-2 fuzzy analytic hierarchy process: The case study of Nigeria. Appl Energy. 2018;228:1853-1869. https://doi.org/10.1016/j.apenergy.2018.07.051

[3] Nedjari Hafida D, Louassa S, Kheder-Haddouche S. MCDM GIS framework for wind energy sites suitability in Algeria's northwest. Energy for Sustainable Development. 2025;89:101836. https://doi.org/10.1016/j.esd.2025.101836
[4] Kaynak T, Gümüş MG. Biogas potential estimation and geospatial decision-making: a hybrid MCDA approach to optimizing biogas facility locations. Environ Dev Sustain. 2025;27(5):12193-12232. https://doi.org/10.1007/s10668-025-06107-5
[5] Atıcı KB, Şimşek AB, Uluçan A, et al. A GIS-based Multiple Criteria Decision Analysis approach for wind power plant site selection. Util Policy. 2015;37:86-96. https://doi.org/10.1016/j.jup.2015.06.001
[6] Özgül C, Taşkanat T, Kaynak T. GIS-supported settlement area determination in post-earthquake reconstruction: an AHP-based suitability analysis in Adıyaman province. Turkish Journal of Remote Sensing. 2025;7(2):407-419. https://doi.org/10.51489/tuzal.1752558
[7] Taşkanat T. Enhancing Artificial Neural Network Performance for Wildfire Susceptibility Mapping Using Bernstein-Levy and Multi-Population Differential Evolution Algorithms. Transactions in GIS. 2026;30(4). https://doi.org/10.1111/tgis.70318
[8] Höfer T, Sunak Y, Siddique H, et al. Wind farm siting using a spatial Analytic Hierarchy Process approach: A case study of the Städteregion Aachen. Appl Energy. 2016;163:222-243. https://doi.org/10.1016/j.apenergy.2015.10.138
[9] Tegou L-I, Polatidis H, Haralambopoulos DA. Environmental management framework for wind farm siting: Methodology and case study. J Environ Manage. 2010;91(11):2134-2147. https://doi.org/10.1016/j.jenvman.2010.05.010
[10] Eroğlu H. A spatial decision making framework using neutrosophic VIKOR for wind energy investment in Turkey. Sci Rep. 2025;15:33593. https://doi.org/10.1038/s41598-025-18799-w
[11] Gyeltshen S, Hayashi K, Mohmmed EEE. Hybrid multi-criteria decision framework for renewable energy site selection: Integrating subjective-objective weighting with PROMETHEE II in climate-vulnerable regions. Energy Reports. 2026;16:109535. https://doi.org/10.1016/j.egyr.2026.109535
[12] Kabak M, Akalın S. A model proposal for selecting the installation location of offshore wind energy turbines. International Journal of Energy and Environmental Engineering. 2022;13:121-134. https://doi.org/10.1007/s40095-021-00421-0
[13] Khalaf OF, Uçan ON, Alsamarai NA. Wind farm sites selection using a machine learning approach and geographical information systems in Türkiye. Discover Computing. 2025;28:22. https://doi.org/10.1007/s10791-025-09511-7
[14] Kesikoglu MH. Comparative analysis of R/SWIR, NIR/SWIR, and NDSI classification methods for determination of snow cover change on Erciyes Mountain, Türkiye using Landsat satellite images. Research on Engineering Structures & Materials. 2025;11(4):1653-1665. https://doi.org/10.17515/resm2025-524ml1110rs
[15] Taşkanat T. Modeling Salinity-Vegetation Interaction in Semi-Arid Areas: A Google Earth Engine Based Comparative Regression Analysis. Turkish Journal of Agricultural and Natural Sciences. 2026;13(2):397-412. https://doi.org/10.30910/turkjans.1844748
[16] Karipoğlu F, Genç MS, Koca K. Determination of the most appropriate site selection of wind power plants based Geographic Information System and Multi-Criteria Decision-Making approach in Develi, Turkey. International Journal of Sustainable Energy Planning and Management. 2021;30:97-114.
[17] Urfalı T, Eymen A. CBS ve AHP yöntemi yardımıyla Kayseri ili örneğinde rüzgâr enerji santrallerinin yer seçimi. Geomatik. 2021;6(3):227-237. https://doi.org/10.29128/geomatik.772453
[18] Kesikoglu MH. Evaluating spatial resolution enhancement on impervious surface detection using support vector machine. Research and Design. 2024;1(1):33-42. https://doi.org/10.17515/rede2024-003bu1111rs
[19] C.L. Cover. Copernicus land monitoring service [Internet]. Eur. Environ, Agency (EEA). 2018 [cited 2026 Jul 22]. Available from: https://land.copernicus.eu/en/products/corine-land-cover/clc2018.
[20] Demir A, Dinçer AE, Çiftçi C, et al. Wind farm site selection using GIS-based multicriteria analysis with Life cycle assessment integration. Earth Sci Inform. 2024;17(2):1591-1608. https://doi.org/10.1007/s12145-024-01227-4
[21] Raja S, Rao R, Shekar S, et al. Application of multi-criteria decision making (MCDM) for site selection of offshore wind farms in India. Operational Research. 2025;25(3):67. https://doi.org/10.1007/s12351-025-00949-7
[22] Raza MA, Yousif M, Hassan M, et al. Site suitability for solar and wind energy in developing countries using combination of GIS-AHP; a case study of Pakistan. Renew Energy. 2023;206:180-191. https://doi.org/10.1016/j.renene.2023.02.010
[23] Chaaban F, Khatib A, Darwishe H. GIS-based spatial modeling and mapping for assessing the suitability of PV solar farm sites in Syria. Discover Applied Sciences. 2026;8:290. https://doi.org/10.1007/s42452-026-08329-2

[24] Elkadeem MR, Younes A, Sharshir SW, et al. Sustainable siting and design optimization of hybrid renewable energy system: A geospatial multi-criteria analysis. Appl Energy. 2021;295:117071. https://doi.org/10.1016/j.apenergy.2021.117071
[25] Farr TG, Rosen PA, Caro E, et al. The Shuttle Radar Topography Mission. Reviews of Geophysics. 2007;45(2):RG2004. https://doi.org/10.1029/2005RG000183
[26] Başeğmez M. A hybrid GIS-fuzzy MCDM and game-theoretic framework for strategic offshore wind farm siting: evidence from the İzmir continental shelf. Expert Syst Appl. 2026;313:131645. https://doi.org/10.1016/j.eswa.2026.131645
[27] Watson JJW, Hudson MD. Regional scale wind farm and solar farm suitability assessment using GIS-assisted multi-criteria evaluation. Landsc Urban Plan. 2015;138:20-31. https://doi.org/10.1016/j.landurbplan.2015.02.001
[28] Yılmaz D, Aslan ŞTA, Vaheddoost B. Gemlik İlçesi rüzgâr enerji santrali potansiyel yer analizi. Geomatik. 2023;8(3):264-276. https://doi.org/10.29128/geomatik.1209940
[29] Latinopoulos D, Kechagia K. A GIS-based multi-criteria evaluation for wind farm site selection. A regional scale application in Greece. Renew Energy. 2015;78:550-560. https://doi.org/10.1016/j.renene.2015.01.041
[30] Al-Yahyai S, Charabi Y, Gastli A, et al. Wind farm land suitability indexing using multi-criteria analysis. Renew Energy. 2012;44:80-87. https://doi.org/10.1016/j.renene.2012.01.004
[31] Sánchez-Lozano JM, García-Cascales MS, Lamata MT. GIS-based onshore wind farm site selection using Fuzzy Multi-Criteria Decision Making methods: Evaluating the case of Southeastern Spain. Appl Energy. 2016;171:86-102. https://doi.org/10.1016/j.apenergy.2016.03.030
[32] Jia W, Zhang Z, Zhou M, et al. Optimal location of slope solid gravity energy storage using geographic information systems and multi-criteria analysis. Energy. 2026;351:140470. https://doi.org/10.1016/j.energy.2026.140470
[33] Triantafyllidou D, Vagiona DG. Enhancing Wind Farm Siting with the Combined Use of Multicriteria Decision-Making Methods. Wind. 2026;6(1):4. https://doi.org/10.3390/wind6010004
[34] Uguz YF, Bilgili A, Uzar M. Toward improved siting of wind-solar hybrid farms: A novel framework integrating multi-criteria decision making, machine learning-driven feature selection, and spatial clustering. Appl Energy. 2026;411:127609. https://doi.org/10.1016/j.apenergy.2026.127609
[35] Workineh TG, Worku GB, Singh SK, et al. A data-driven geographic information system and machine learning based multi-criteria framework for strategic wind power plant siting. Sci Rep. 2026;16. https://doi.org/10.1038/s41598-026-51265-9
[36] Tekin S, Guner ED, Cilek A, et al. Selection of renewable energy systems sites using the MaxEnt model in the Eastern Mediterranean region in Turkey. Environmental Science and Pollution Research. 2021;28(37):51405-51424. https://doi.org/10.1007/s11356-021-13760-6
[37] Ayar B, Yalçın Z, Dağ M. Harvesting the wind: A study on the feasibility and advancements of wind energy potential using distribution functions. Avrupa Bilim ve Teknoloji Dergisi. 2023;(23):173-182.
[38] Mera Kanunu [Internet]. T.C. Resmî Gazete, 4342 Türkiye Cumhuriyeti; Feb 28, 1998. Available from: https://www.resmigazete.gov.tr/.
[39] SHGM. Haberleşme, Seyrüsefer, Gözetim Sistemleri Mânia Kriterleri Hakkında Yönetmelik [Internet]. T.C. Resmî Gazete, 28451 Oct 24, 2012. Available from: https://web.shgm.gov.tr/doc5/mk.pdf.
[40] T.C. ETKB. Frequently Asked Questions, "How is site selection performed for licensed wind power plants? [Internet]. T.C. ETKB. 2026 [cited 2026 Sep 22]. Available from: https://enerji.gov.tr/sikca-sorulan-sorular.
[41] TEİAŞ. Türkiye Elektrik İletim A.Ş. 2026 Yılı İçin Dağıtım Seviyesinden Transformatör Merkezi Bazlı Tahsis Edilen Güneş ve Rüzgar Kaynaklı Kalan Lisanssız Üretim Kapasiteleri [Internet]. TEİAŞ. 2026 [cited 2026 Jul 22]. Available from: https://www.teias.gov.tr/duyurular/2026-yili-icin-dagitim-seviyesinden-transformator-merkezi-bazli-tahsis-edilen-gunes-ve-ruzgar-kaynakli-kalan-lisanssiz-uretim-kapasiteleri-16072026.